IGFBP-3 Mediates Metabolic Homeostasis During Hyperosmolar Stress in the Corneal Epithelium

Evan D. Bogdan, Whitney L. Stuard, Rossella Titone, and Danielle M. Robertson

Department of Ophthalmology, UT Southwestern Medical Center, Dallas, Texas, United States

Correspondence: Danielle M. Robertson, Department of Ophthalmology, UT Southwestern Medical Center, 5323 Harry Hines Blvd., Dallas, 75390-9057 TX, USA; danielle.robertson@utsouthwestern.edu.

Received: September 16, 2020
Accepted: April 21, 2021
Published: June 8, 2021

Citation: Bogdan ED, Stuard WL, Titone R, Robertson DM. IGFBP-3 mediates metabolic homeostasis during hyperosmolar stress in the corneal epithelium. *Invest Ophthalmol Vis Sci.* 2021;62(7):11. https://doi.org/10.1167/iovs.62.7.11

Purpose. The insulin-like growth factor binding protein-3 (IGFBP-3) is a multifunctional secretory protein with well-known roles in cell growth and survival. Data in our laboratory suggest that IGFBP-3 may be functioning as a stress response protein in the corneal epithelium. The purpose of this study is to determine the role of IGFBP-3 in mediating the corneal epithelial cell stress response to hyperosmolarity, a well-known pathophysiological event in the development of dry eye disease.

Methods. Telomerase-immortalized human corneal epithelial (hTCEpi) cells were used in this study. Cells were cultured in serum-free media with (growth) or without (basal) supplements. Hyperosmolarity was achieved by increasing salt concentrations to 450 and 500 mOsM. Metabolic and mitochondrial changes were assessed using Seahorse metabolic flux analysis and assays for mitochondrial calcium, polarization and mtDNA. Levels of IGFBP-3 and inflammatory mediators were quantified using ELISA. Cytotoxicity was evaluated using a lactate dehydrogenase assay. In select experiments, cells were cotreated with 500 ng/mL recombinant human (rh)IGFBP-3.

Results. Hyperosmolar stress altered metabolic activity, shifting cells towards a respiratory phenotype. Hyperosmolar stress further altered mitochondrial calcium levels, depolarized mitochondria, decreased levels of ATP, mtDNA, and expression of IGFBP-3. In contrast, hyperosmolar stress increased production of the proinflammatory cytokines IL-6 and IL-8. Supplementation with rhIGFBP-3 abrogated metabolic and mitochondrial changes with only marginal effects on IL-8.

Conclusions. These findings indicate that IGFBP-3 is a critical protein involved in hyperosmolar stress responses in the corneal epithelium. These data further support a new role for IGFBP-3 in the control of cellular metabolism.

Keywords: corneal epithelial cells, mitochondria, respiration, glycolysis, hyperosmolarity, inflammation

Dry eye disease is one of the most common ocular conditions worldwide.[1] One of the central pathophysiological features of dry eye is hyperosmolarity of the precorneal tear film.[2–4] An increase in tear osmolarity occurs when the lacrimal gland fails to produce enough aqueous to bathe the eye or when there is a deficiency in the lipids that are required to stabilize the tear film, leading to evaporation of the watery aqueous.[2,5] This increase in osmolarity activates toll-like receptors along with water and ion channels that drive activation of mitogen-activated protein kinase pathways.[6–11] This in turn triggers a circuitous cascade of proinflammatory mediators and matrix metalloproteinases, leading to ocular surface damage.[7, 12–19] Using various cell culture models, previous studies have shown that hyperosmolar culture is also associated with an increase in oxidative stress, mitochondrial dysfunction, and apoptosis.[15,16,20–23] Moreover, recent studies have suggested that autophagic flux may be altered in dry eye disease.[24]

The insulin-like growth factor binding protein-3 (IGFBP-3), is a multifunctional protein with known roles in cell growth and programmed cell death.[25–31] IGFBP-3 is one of six IGFBPs in the insulin-like growth factor (IGF) superfamily. IGFBP-3 is the most predominant binding protein in serum.[32] As such, the canonical function of IGFBP-3 is to extend the half-life of IGF-1 in circulation and to inhibit binding of IGF-1 to the type 1 IGF receptor (IGF-1R).[32,33] IGFBP-3 can also function independently of IGF-1 and potential cell surface receptors for IGFBP-3 have been reported.[33–36] Our laboratory identified IGFBP-3 in human tear fluid and found that it was increased almost 3 fold in patients with type 2 diabetes mellitus.[37–39] We have also found that IGFBP-3 is upregulated by corneal epithelial cells in response to stress induced by growth factor withdrawal.[40] More recently, we identified a novel role for IGFBP-3 in mediating mitophagy and mitochondrial biogenesis, key mitochondrial quality control mechanisms in corneal epithelial cells (Stuard WL, Titone R, and Robertson DM, manuscript in review, 2021).

In nonocular tissues, enhanced expression of IGFBP-3 has been shown to exert an anti-inflammatory effect.[41–43] On the basis of these findings and the novel role for IGFBP-3 in mediating mitochondrial homeostasis, we posited that IGFBP-3 may function as a critical stress response protein in the corneal epithelium. Here we show that hyperosmolar

culture induces significant metabolic abnormalities that are associated with a loss of IGFBP-3. We further demonstrate that the addition of exogenous IGFBP-3 can abrogate these metabolic effects, supporting a new role for IGFBP-3 in the control of cellular metabolism.

Methods

Cell Culture

A human telomerized corneal epithelial (hTCEpi) cell line previously developed and characterized by our laboratory was used for these studies.[44] hTCEpi cells were cultured in serum-free keratinocyte basal medium (KBM) containing 0.06 mM calcium supplemented to 0.15 mM (VWR, Radnor, PA, USA), 6 mM glucose, and additional supplements: bovine pituitary extract (0.0004 mL/mL), recombinant human epidermal growth factor (0.125 ng/mL), recombinant human insulin (5 µg/mL), hydrocortisone (0.33 µg/mL), epinephrine (0.39 µg/mL), and human holotransferrin (10 µg/mL, PromoCell; VWR). Media with supplements is defined as keratinocyte growth media (KGM). For all experiments, cells were cultured at 37°C in 5% CO_2. Based on manufacturer data, osmolarity of KGM is approximately 330 mOsM. Hyperosmolar stress was induced by the addition of NaCl (Thermo Fisher, St. Louis, MO, USA) to culture media to reach 450 mOsM and 500 mOsM. In select experiments, cells exposed to hyperosmolar culture were co-treated with 500 ng/mL recombinant human (rh)IGFBP-3 (Sino Biological, Wayne, PA, USA).

Determination of Cell Number

hTCEpi cells were seeded in KGM or KBM at 70-80% confluence in 6-well tissue culture plates and cultured overnight. Media was then removed and replaced with isotonic KGM or KGM supplemented with each concentration of NaCl as described and cultured for an additional 24 hours. Cells were imaged by phase contrast microscopy using a Leica DM inverted microscope equipped with a DFC3000 G camera (Leica Microsystems, Heidelberg, Germany). Cell counts were obtained using a Celigo imaging cytometer (Nexcelom, Lawrence, MA, USA). All cell counts were performed in triplicate and repeated a minimum of two additional times.

Cell Proliferation Assay

To assess cell proliferation, hTCEpi cells were seeded in KGM or KBM at 3×10^4 cells per well in a 96-well, black-walled tissue culture plate and grown overnight. Media was subsequently removed and replaced with isotonic KGM, KBM, or either media supplemented with NaCl to 450 or 500 mOsM. Cells were incubated in hyperosmolar conditions for six or 24 hours, as indicated. Cellular DNA content was measured via fluorescent dye binding using a CyQuant NF Cell Proliferation Assay Kit (Invitrogen, Carlsbad, CA, USA). Fluorescent signals were detected using a Synergy 2 Multi-Mode Microplate Reader (BioTek, Winooski, VT, USA) with excitation at 485 nm and emission at 530 nm. All samples were plated in eight replicate wells. Each experiment was repeated a minimum of two additional times.

ELISA

The levels of intracellular and secreted IGFBP-3 were measured using ELISA. To measure intracellular levels, cells were lysed using radioimmunoprecipitation buffer containing a protease and phosphatase inhibitor cocktail (Thermo Fisher). Lysates were then spun in a centrifuge at 12,000 rpm for five minutes at 4°C. To measure secreted protein, conditioned media was concentrated using iCON protein concentrators (MW cutoff 3K; Millipore, Burlington, MA, USA). Total protein was measured using a QuBit 3.0 Fluorometer (Thermo Fisher). A solid phase sandwich ELISA was used to quantify IGFBP-3 levels (human Quantikine ELISA; R&D Systems, Minneapolis, MN, USA). Recombinant human IGFBP-3 protein was used as a standard control. ELISA plates were imaged using a BioTek Synergy multi-mode plate reader (BioTek). The concentration of IGFBP-3 in conditioned media was normalized to total cell lysate protein. The concentration of IGFBP-3 in cell lysates was normalized to β-actin measured by densitometry on a western blot. ELISA was also used to measure levels of IL-6 and IL-8. Conditioned media was concentrated as above. Human IL-6 and human IL-8/CXCL8 Quantikine ELISAs (R&D Systems) were used to quantify levels in media. All experiments were performed in triplicate and repeated a minimum of two additional times.

Cell Cycle Determination

For cell cycle assays, 6×10^5 cells were seeded onto 6-well tissue culture plates and cultured in KGM or KBM with increasing concentrations of salt. Cells were fixed using ice cold ethanol for 15 minutes at 4°C and then stained with 300 µg/mL propidium iodide containing RNase (Cell Signaling, Danvers, MA, USA). After washing with PBS, cells were imaged using a Celigo imaging cytometer (Nexcelom). Cell cycle analysis was performed using the manufacturer provided software. Each experiment was performed in triplicate and repeated a minimum of two additional times.

Real-Time Metabolic Studies

Real-time measurements of cellular oxygen consumption rate (OCR) and extracellular acidification rate (ECAR) were performed simultaneously using a Seahorse Metabolic Flux Analyzer XFp (Agilent Technologies, Santa Clara, CA). hTCEpi cells were seeded in KGM at 30,000 cells per well in Seahorse mini-plates containing 8 wells (Agilent Technologies) and cultured overnight. Media was subsequently removed from each plate and replaced with isotonic KGM (330 mOsM), or KGM supplemented with NaCl to an osmolarity of 450 mOsM and 500 mOsM. Cells were then incubated for 24 hours under isotonic or hyperosmolar conditions. After 24 hours, hyperosmotic media was removed and replaced with Seahorse XF DMEM medium containing 1 mM sodium pyruvate, 2 mM glutamine, 10 mM glucose, and 5 mM HEPES without phenol red (pH 7.4, Agilent Technologies). Cells were incubated in this medium for one hour at 37°C in a standard non-CO_2 incubator, after which this medium was replaced with fresh Seahorse XF medium just before analysis. OCR, a marker for mitochondrial respiration, and ECAR, a marker for glycolysis, were analyzed using a Seahorse XFp Cell Mito Stress Test Kit or a Seahorse XFp Real Time ATP Rate Assay (Agilent Technologies). All assays were performed according to manufacturer instructions, as briefly described below. For quantitation of metabolic

Investigative Ophthalmology & Visual Science

activities using the Seahorse XFp Cell Mito Stress Test Kit, 10 µM oligomycin was injected to inhibit ATP synthase at 20 minutes, allowing for measurement of mitochondrial respiration associated with cellular ATP production. At 50 minutes, 5 µM carbonyl cyanide 4-(trifluoromethoxy) phenylhydrazone was injected to disrupt the mitochondrial membrane potential by collapsing the proton gradient, allowing for measurement of maximal oxygen consumption because of uninhibited electron flow through the electron transport chain. At 80 minutes, 5 µM rotenone/antimycin A was injected to completely inhibit mitochondrial respiration, allowing for measurement of non-mitochondrial respiration. Measurements were obtained every six to seven minutes for a total of 94 minutes. For the Seahorse XFp Real-Time ATP Rate Assay Kit, only two injections were performed, the first injecting 15 µM oligomycin at 20 minutes and the second injecting 5 µM rotenone/antimycin A at 40 minutes. Similarly, measurements were obtained in real time every six to seven minutes for a total of 74 minutes. Data were analyzed using the manufacturer provided Wave software, version 2.3.0. The ratio for OCR/ECAR was calculated for each experiment. All samples were plated in 6 replicate wells. OCR, ECAR, and ATP levels were all normalized to total cell number using a Celigo imaging cytometer (Nexcelom). Each experiment was repeated a minimum of two additional times.

Rhod-2 Calcium Assay

To assess levels of mitochondrial calcium, hTCEpi cells were seeded in KGM or KBM at a concentration of 3×10^4 cells/well in a 96-well, black-walled tissue culture plate and grown overnight. Media was then removed from each well and replaced with standard isotonic KBM (330 mOsm), or KBM with increasing osmolarity. Cells were incubated for 24 hours. Calcium levels were measured using a fluorescence assay containing the cell permeable mitochondrial calcium indicator rhod-2 (Thermo Fisher). Rhod-2 was dissolved in dimethyl sulfoxide (Sigma, St. Louis, MO, USA) to a concentration of 2 mM and then diluted in KGM to a final working concentration of 2 µM. N,N,N′,N′-*tetrakis*-2-Pyridylmethylethylenediamine (Sigma, St. Louis), a heavy metal-selective chelator, was also added at a final concentration of 50 µM to prevent rhod-2 nonselective binding of heavy metal cations. Cells were incubated in this solution for 30 minutes at 37˚C, washed, and subjected to a second incubation in hyperosmolar culture for an additional 30 minutes at 37˚C. Fluorescence was then measured using a Synergy 2 Multi-Mode Microplate Reader (BioTek) with excitation at 552 nm and emission at 581 nm. Data was then normalized for cell number using a K2 Cellometer (Nexcelom). Eight wells were plated for each sample per experiment. Each experiment was repeated a minimum of two additional times.

JC-1 Staining

To determine the effects of hyperosmolarity on mitochondrial polarization, 9×10^4 hTCEpi cells were plated on coverslip bottom MatTek dishes (MatTek Corporation, Ashland, MA, USA) and allowed to attach. Cells were cultured in growth media with increasing concentrations of salt and incubated for 24 hours. Cells were then labelled with 10 µg/mL of tetraethyl-benzimidazolylcarbocyanine iodide (JC-1) dye (Invitrogen/Molecular Probes, Eugene, OR, USA). For a positive control for depolarization, cells were treated with the oxidative phosphorylation uncoupler, carbonyl cyanide *m*-chlorophenyl hydrazine (CCCP, 50 nM), in dimethyl sulfoxide for 10 minutes at 37°C. Cells were then washed with PBS. JC-1 staining was visualized using a Leica SP8 laser scanning confocal microscope (Leica Microsystems, Heidelberg, Germany) with a 63 × oil objective. The microscope is equipped with an environmental chamber to maintain cells at 5% CO_2 and 37°C during imaging. JC-1 monomers were scanned using a 488 nm excitation laser and JC-1 aggregates were scanned using a 561 nm excitation laser. Sequential scanning was performed to prevent spectral crosstalk. Imaging experiments were repeated an additional two times.

Western Blotting

Intracellular levels of IGFBP-3 were measured using western blotting. Cell lysates were harvested as described above and measured using a QuBit 3.0 Fluorometer (Thermo Fisher). After centrifugation of cell lysates, supernatants were boiled in 2× sample buffer containing 65.8 mM Tris-HCL, 26.3% (w/v) glycerol, 2.1% sodium dodecyl sulfate, 5.0% β-mercaptoethanol and 0.01% bromophenol blue, pH 6.8 (Bio-Rad, Hercules, CA, USA). Samples were then electrophoresed in a 4% to 15% precast linear gradient polyacrylamide gel (Bio-Rad) and then transferred to a polyvinyl difluoride membrane (Millipore). After blocking in 5% nonfat milk (Bio-Rad), membranes were incubated at 4°C in a primary antibody against IGFBP-3 (mouse monoclonal; R&D Systems) overnight, followed by one hour in anti-mouse secondary antibody. β-actin (mouse monoclonal; Sigma) was used as a loading control. Proteins were visualized using ECL Prime Detection Reagent (Amersham Biosciences, Piscataway, NJ, USA) and imaged using an Amersham Imager 600 (Amersham Biosciences).

mtDNA Imaging

SYBR green (Thermo Fisher Scientific, Waltham, MA, USA) was used to label mtDNA as described.[45] In total, 9×10^4 hTCEpi cells were plated on coverslip bottom MatTek dishes and allowed to adhere overnight. Cells were then cultured in isotonic basal media or basal media supplemented to 450 mOsM with or without rhIGFBP-3. Cells were stained with a 1:10,000,000 dilution of SYBR green for 10 minutes at 37°C. MtDNA was visualized using a Leica SP8 laser scanning confocal microscope with a 63 × oil objective inside an environmental chamber. Cells were scanned using a 488 nm excitation laser. Imaging experiments were repeated an additional two times.

Cytotoxicity Assay

Cytotoxicity was quantified using a CyQuant lactate dehydrogenase (LDH) cytotoxicity assay (Thermo-Fisher Scientific, Waltham, MA). The assay was performed according to manufacturer instructions. Briefly, cells were seeded in a 96-well plate and incubated overnight. Cells were then treated with ultrapure water to determine spontaneous LDH activity, lysis buffer to determine the maximum LDH release, or nothing was added to determine the maximum LDH activity. Cells were again incubated in each of the three conditions for 45 minutes. Samples were mixed with the reaction mixture for 30 minutes, followed by the stop solution. Absorbance was read at 490 nm and 680 nm. Cells were plated in triplicate for each treatment condition and the entire experiment was repeated at least two additional times.

Investigative Ophthalmology & Visual Science

Statistical Analysis

All data are expressed as mean ± standard deviation. Normality was assessed using a Shapiro-Wilks test. For comparison between groups, a one-way ANOVA was used with an appropriate post-hoc comparison (Holm-Sidak method or Student-Newman Kheuls test). Statistical significance was set at $P < 0.05$.

Results

To determine the effect of hyperosmolarity on cell division in hTCEpi cells, cells were cultured in basal media subject to increasing levels of hyperosmolar stress for 6 or 24 hours. As shown in Figure 1A, six hours of hyperosmolar culture had no effect on overall cell number compared to cells in the isotonic condition ($P = 0.093$). In contrast, by 24 hours, cell number was decreased in a stepwise fashion with increasing osmolarity (Fig. 1B, $P < 0.001$). These findings were consistent with the decrease in cell number observed by phase contrast microscopy in growth media (Supplementary Fig. S1A). Likewise, quantification of cell number in growth media using a CyQuant assay confirmed the salt concentration dependent effect, whereby each increase in hyperosmolarity further reduced the amount of measurable DNA (Supplementary Fig. S1B, $P < 0.001$).

To determine how hyperosmolarity regulates cell proliferation in hTCEpi cells, cell cycle was analyzed using propidium iodide-stained cells. After six hours of hyperosmolar culture, cells arrested in G2/M (Fig. 1C, $P < 0.001$ for 450 compared to KBM and 500 compared to KBM). There was a slight, but significant increase in the percentage of cells arrested in the 500 mOsM/kg condition compared to 450 mOsM/kg ($P = 0.044$). The G2/M arrest was not evident at 24 hours (Fig. 1D). Instead, there was a significant decrease in the percentage of cells in hyperosmolar culture in the G2/M phase, while cells appeared to be accumulating in the G0/G1 phase ($P < 0.001$ for 450 compared to KBM and for 500 compared to KBM). At 24 hours, there were no significant differences between the two hyperosmolar conditions.

We next investigated metabolic changes in response to hyperosmolarity in basal media. Using a Cell Mito Stress test, we found a significant reduction in the extracellular acidification rate in both hyperosmolar conditions at the 6-hour time point (Fig. 2A, $P < 0.021$ for 450 mOsM compared to KBM and $P < 0.001$ for 500 mOsM compared to KBM). Although mitochondrial respiration was not significantly decreased after six hours of culture at 450 mOsM, it was decreased at 500 mOsM ($P < 0.001$). After 24 hours of culture in basal media, both glycolysis and respiration were decreased in hyperosmolar culture ($P < 0.001$ for both respiration and glycolysis at 450 mOsM compared to KBM), with a greater reduction seen in the 500 mOsM condition (Fig. 2B, $P = 0.035$ and $P = 0.017$ for respiration and glycolysis, respectively). Analysis of the metabolic phenotype revealed no changes at 6 hours (Fig. 2C, $P = 0.248$). At 24 hours however, there was a progressive shift towards a respiratory phenotype with increasing osmolarity (Fig. 2D, $P = 0.005$). Consistent with the reduction in respiration that was evident in the 500 mOsM group at six hours, there was a similar decrease in ATP (Fig. 2E, $P < 0.001$). Likewise, at 24 hours, there was a sequential decrease in ATP production at 450 mOsM and 500 mOsM (Fig. 2F, $P < 0.001$ and $P = 0.017$ for 450 and 500 compared to KBM and 500 compared to 450, respectively). Importantly, the six-hour effect on glycolysis in cells cultured at 450 mOsm in basal media mirrored what was seen after 24 hours in growth media (Supplementary Fig. S2). These findings suggest that additional components in the growth media afforded some level of protection against mitochondrial compromise in the milder salt condition.

To further examine the effects of hyperosmolar culture on mitochondria, we next measured the concentration of mitochondrial calcium using the mitochondrial calcium indicator rhod-2. Consistent with the mitochondrial respiration response, there was no change in mitochondrial calcium in the 450 mOsM group at 6 hours, whereas there was a significant decrease in cells cultured in 500 mOsM (Fig. 3A, $P < 0.05$ compared to KBM). After culture for 24 hours, there was an unexpected increase in mitochondrial calcium at 450 mOsM, which was significantly reduced in the 500 mOsM condition (Fig. 3B, $P < 0.05$). In growth media, while mitochondrial calcium levels trended higher at 450 mOsM, this was not significant compared to cells cultured in KGM. At 500 mOsM, mitochondrial calcium was significantly increased compared to KGM and 450 mOsM (Supplementary Fig. 3A, $P < 0.001$). Similarly, using the membrane permeable MitoProbe JC-1, hyperosmolar stress induced robust mitochondrial depolarization in growth media containing 500 mOsM, while only mild to moderate depolarization was evident in the 450 mOsM condition (Supplementary Fig. S3B). In this latter condition, some mitochondria appeared more elongated, suggestive of active respiration. At 500 mOsM, mitochondria no longer showed their elongated tubular network, but were beginning to show evidence of fragmentation. As expected, cells treated with the uncoupler of oxidative phosphorylation showed complete depolarization and fragmentation.

We next examined the effects of hyperosmolarity on IGFBP-3 secretion in basal media. Treatment with both 450 mOsM and 500 mOsM significantly decreased IGFBP-3 secretion, with almost complete inhibition at the latter osmolarity (Fig. 4A, $P < 0.001$). Immunoblotting was then used to examine intracellular levels of IGFBP-3 (Fig. 4B). Again, both salt concentrations decreased expression of IGFBP-3, with the greatest effect seen at 500 mOsM. Consistent with this, cells cultured in growth media also showed a decrease in intracellular levels of IGFBP-3 in response to hyperosmolar stress (Supplementary Fig. S4). In this test condition, increasing hyperosmolarity to 450 mOsM decreased intracellular IGFBP-3 levels by half ($P < 0.001$ compared to the KGM control). Further increasing the salt concentration to 500 mOsM did not result in a further reduction in the already low level of IGFBP-3 ($P < 0.001$ compared to the KGM control). We then tested the effects of co-treatment with rhIGFBP-3 on mitochondrial respiration and glycolysis during hyperosmolar culture. As shown in Figure 4C, co-treatment with rhIGFBP-3 blocked the hyperosmolar mediated decrease in glycolysis and respiration ($P = 0.042$ and $P = 0.012$ for differences in respiration and glycolysis between IGFBP-3 treated cells and 450 mOsM). Co-treatment with rhIGFBP-3 also maintained the bioenergetic profile in a more glycolytic state, demonstrated by the ratio of oxygen consumption to glycolysis (Fig. 4D). Staining of mtDNA showed a reduction in mtDNA in 450 mOsM that was blocked by rhIGFBP-3 (Fig. 4E).

Hyperosmolar induced inflammation is a key step in the pathogenesis of dry eye. To determine whether IGFBP-3 mediates inflammation, we examined the production of

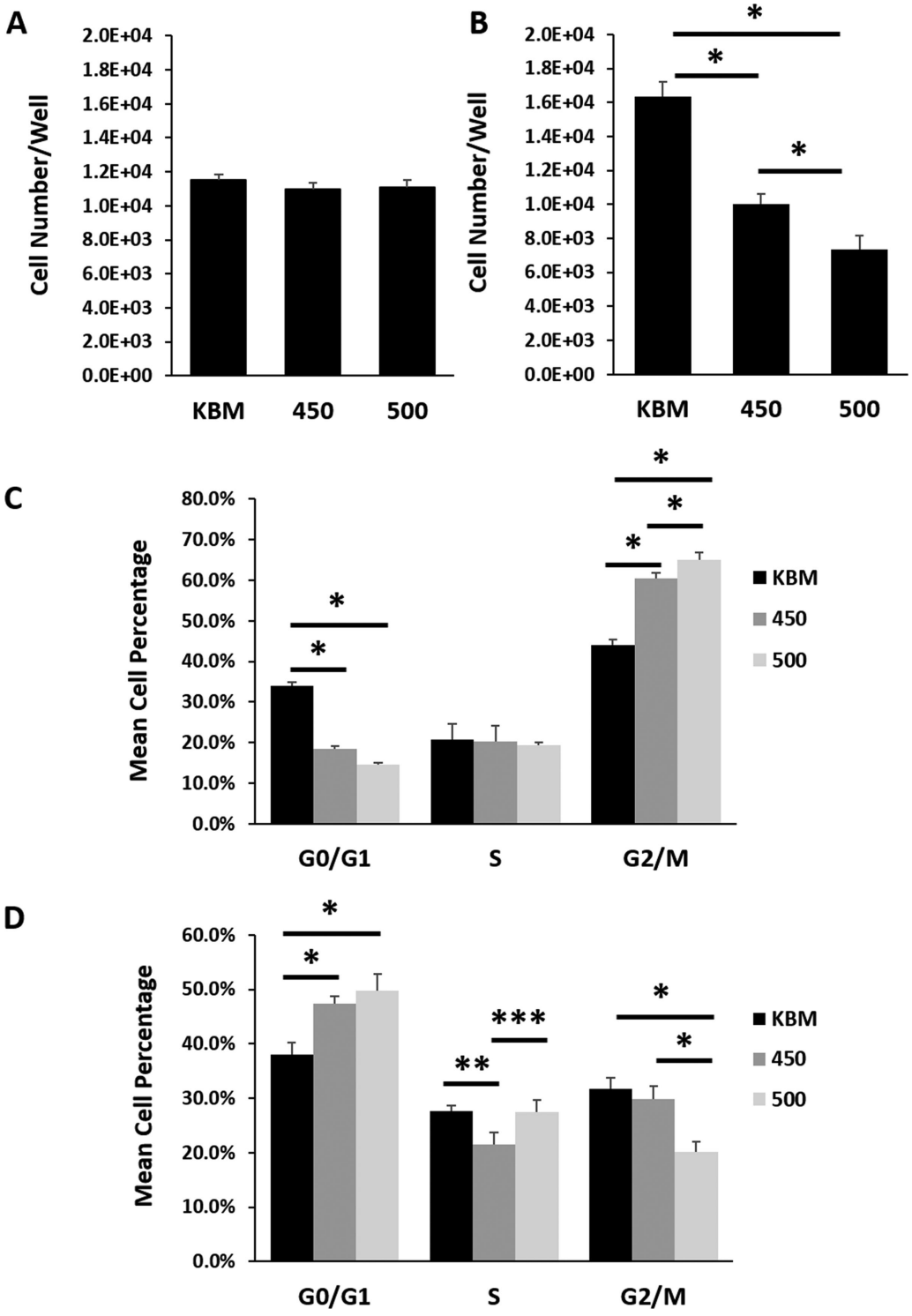

Figure 1. Hyperosmolarity induced a biphasic arrest in corneal epithelial cells. hTCEpi cells were cultured in basal media with increasing concentrations of salt. Cell number and cell cycle were assessed at six and 24 hours. (**A**) There were no differences in cell number between any of the test conditions at six hours ($P = 0.093$, one-way ANOVA, n = 3). (**B**) After 24 hours, there was a progressive decrease in cell number with increasing osmolarity ($^{*}P < 0.001$, one-way ANOVA, SNK multiple comparison test, n = 3). (**C**) After six hours in hyperosmolar culture, hTCEpi cells were arrested at G2/M ($^{*}P < 0.001$, $^{**}P = 0.044$, one-way ANOVA, SNK multiple comparison test, n = 3). (**D**) At 24 hours, hTCEpi cells cultured under hyperosmolar conditions were arrested in G0/G1 ($^{*}P < 0.001$, $^{***}P = 0.004$, $^{****}P = 0.002$, one-way ANOVA, SNK multiple comparison test, n = 3). Data represented as mean ± standard deviation. Graphs representative of a single experiment repeated 3 times. KBM, keratinocyte basal media. Number indicates mOsM.

Investigative Ophthalmology & Visual Science

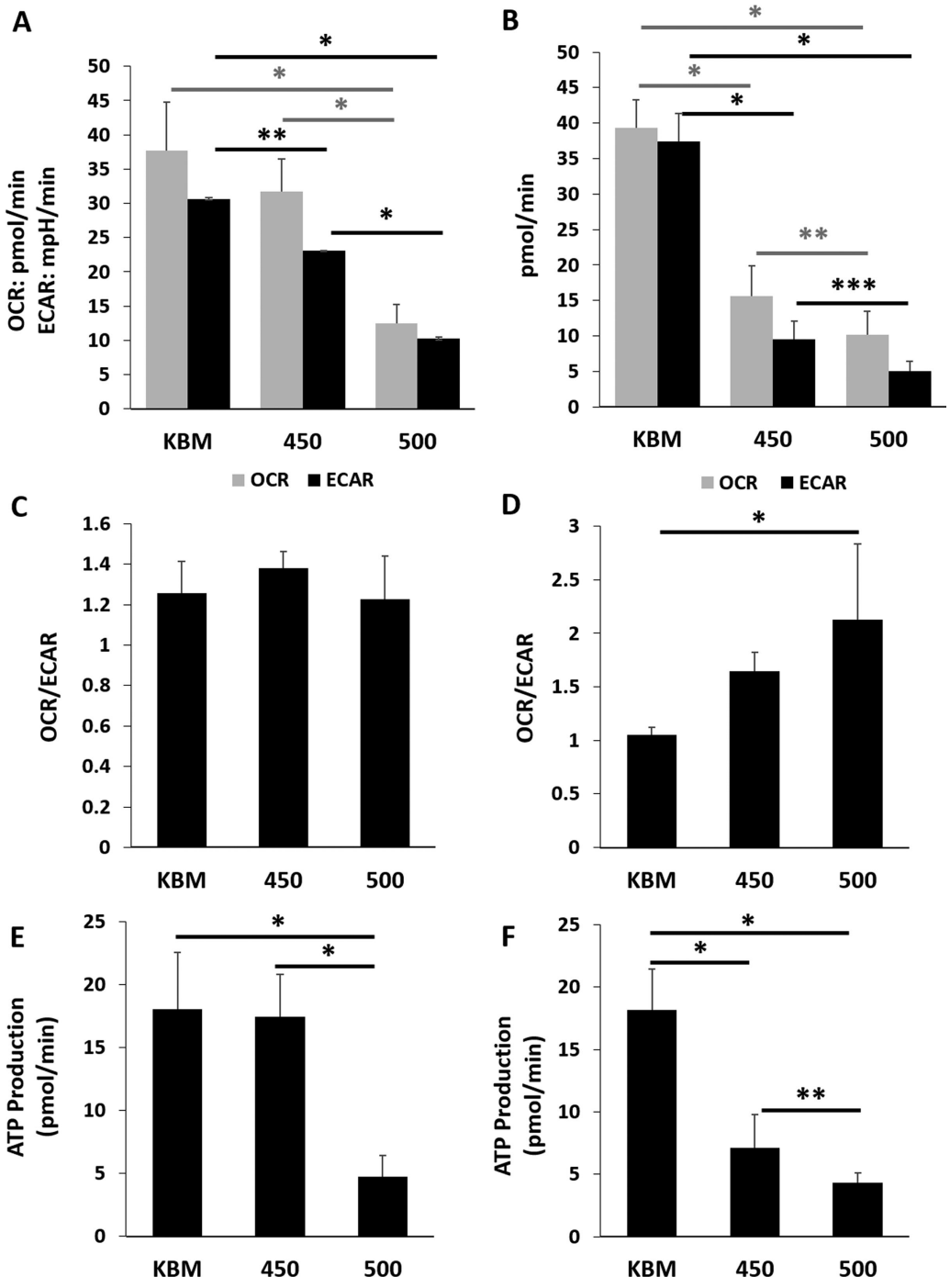

Figure 2. Hyperosmolar stress decreases both mitochondrial respiration and glycolysis in corneal epithelial cells. The hTCEpi cells were cultured in basal media with increasing concentrations of salt. Metabolism was measured using a Seahorse metabolic flux analyzer after six and 24 hours of hyperosmolar culture. (**A**) At six hours of culture in 450 mOsM, glycolysis was significantly decreased compared to the basal control ($^{**}P = 0.021$). It was further decreased with 500 mOsM ($^{*}P < 0.001$). In contrast to this, respiration was not altered after six hours in 450 mOsM but was significantly decreased in 500 mOsM ($^{*}P < 0.001$, one-way ANOVA, SNK multiple comparison test, n = 3). (**B**) After 24 hours of culture, glycolysis was severely attenuated in hyperosmolar culture ($^{*}P < 0.001$, $^{****}P = 0.017$, one-way ANOVA, SNK multiple comparison test, n = 3). Mitochondrial respiration was similarly decreased ($^{*}P < 0.001$, $^{***}P = 0.035$, n = 3). (**C**) There were no differences in the OCR/ECAR ratio at six hours ($P = 0.248$, one-way ANOVA, SNK multiple comparison test, n = 3). (**D**) hTCEpi cells expose to increased osmolarity shifted towards a more respiratory phenotype ($P = 0.0005$, one-way ANOVA, SNK multiple comparison test, n = 3). (**E**) ATP production was decreased after six-hour culture in 500 mOsM ($^{*}P < 0.001$, one-way ANOVA, SNK multiple comparison test, n = 3). (**F**) After 24 hours, ATP production was decreased in both the 450 mOsM and 500 mOsM test groups ($^{*}P < 0.001$). The greater osmolarity was associated with a greater decrease in ATP production ($^{****}P = 0.017$, one-way ANOVA, SNK multiple comparison test, n = 3). Data represented as mean ± standard deviation. Graphs representative of a single experiment repeated three times. Number indicates mOsM.

Investigative Ophthalmology & Visual Science

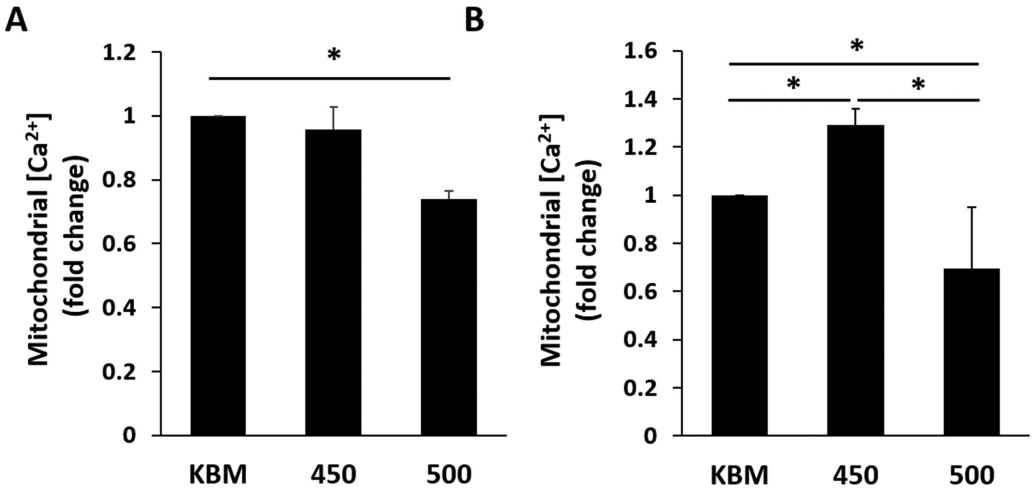

Figure 3. Hyperosmolar stress induces differential shifts in mitochondrial calcium in corneal epithelial cells cultured in basal media. The hTCEpi cells were cultured in basal media with increasing concentrations of salt for six or 24 hours. (A) Mitochondrial calcium was decreased after six hours of culture in 500 mOsM ($^*P < 0.05$, one-way ANOVA, SNK multiple comparison test, n = 3). (B) After 24 hours of culture, mitochondrial calcium was increased in 450 mOsM, but decreased in 500 mOsM ($^*P < 0.05$, one-way ANOVA, SNK multiple comparison test, n = 3). Data represented as mean ± standard deviation. Graphs representative of a single experiment repeated 3 times. Number indicates mOsM.

IL-6 and IL-8 by hTCEpi cells. After 24 hours of hyperosmolar stress, both IL-6 and IL-8 were significantly increased in 450 mOsM compared to the isotonic basal control (Fig. 5, $P = 0.008$ and $P = 0.001$ for IL-6 and IL-8, respectively). Co-treatment with rhIGFBP-3 had no effect on IL-6 levels (Fig. 5A), but resulted in a partial reduction in IL-8 (Fig. 5B, $P = 0.033$). Last, to confirm that there was no significant cytotoxicity that may impact findings, cytotoxicity was measured using an LDH assay. Importantly, although there was a statistical increase in LDH release in cells cultured in 450 mOsM of salt, overall cytotoxicity remained around 5% for cells with and without IGFBP-3 (Supplementary Fig. S5).

Discussion

The first key finding in this study is that hyperosmolar stress targets the glycolytic pathway before impacting mitochondrial respiration. This disproportionate decrease in glycolysis compared to respiration resulted in a metabolic shift toward a respiratory phenotype. This shift was somewhat attenuated in growth media, suggesting that the factors in growth media conferred some protection. We have previously shown that insulin promotes mitochondrial polarization and respiration in corneal epithelial cells and is essential in preventing mitochondrial fragmentation in response to certain types of mild stress.[46] Based on that data, we speculate that the presence of insulin in growth media aided in the maintenance of polarization and respiration in the presence of mild hyperosmolar stress. The beneficial effects of insulin were subsequently lost when the salt concentration reached 500 mOsM.

At a metabolic level, it is well established that corneal epithelial cells are highly glycolytic and can regulate respiration and glycolysis depending on their energy demand.[47,48] Although some studies have indicated mitochondrial damage in hyperosmolar culture through the release of cytochrome c and cell death, little is known about the effects of increased salt concentration on glycolysis in this cell type. In cerebellar granule cells, hyperosmolar stress induced by increasing the concentration of NaCl has been shown to trigger a reduction in glycolysis.[49] This is followed by a decrease in ATP generation and subsequent necrosis. In the present study, the early reduction in glycolysis was not sufficient to drive a decrease in ATP because of the compensatory role of mitochondrial respiration. This compensatory effect was not maintained at the higher salt concentration because of widespread mitochondrial depolarization and subsequent morphological changes.

The second key finding in this study is the robust downregulation of IGFBP-3 in response to hyperosmolar stress. Importantly, this finding was evident in both growth and basal media. Based on our prior data, we had anticipated an upregulation of IGFBP-3, similar to our hyperglycemic cultures.[50] Because IGFBP-3 has well-known roles in growth downregulation and apoptosis,[31] the decrease in IGFBP-3 from hyperosmolar stress ruled out a role for IGFBP-3 mediated growth arrest or the induction of apoptosis. Instead, supplementation with rhIGFBP-3 blocked the onset of any metabolic abnormalities. Although the mechanism by which IGFBP-3 mediates metabolism in corneal epithelia is unknown, the potential for IGFBP-3 to regulate nuclear gene expression remains a viable pathway. We have previously shown that IGFBP-3 induces nuclear translocation of the insulin-like growth factor-1/insulin receptor hybrid (Hybrid-R) in corneal epithelial cells where it interacts with nuclear DNA.[51,52] Consistent with this finding, nuclear localized IGF-1R has been shown to mediate transcription in multiple cell types.[53–55] Thus further studies are needed to elucidate the relationship between nuclear translocation of the Hybrid-R and metabolic control.

As indicated above, mitochondrial changes have been reported to occur in corneal epithelial cells in response to hyperosmolar stress. Luo and colleagues used primary cultured corneal epithelial cells to show that hyperosmolar culture induced apoptosis by triggering the release of cytochrome c.[20] Png et al.[21] also investigated the effect of hyperosmolar stress on corneal epithelial cells. In this latter study, they showed that culture of SV40 corneal epithelial cells in hyperosmolar conditions resulted in a loss of

Investigative Ophthalmology & Visual Science

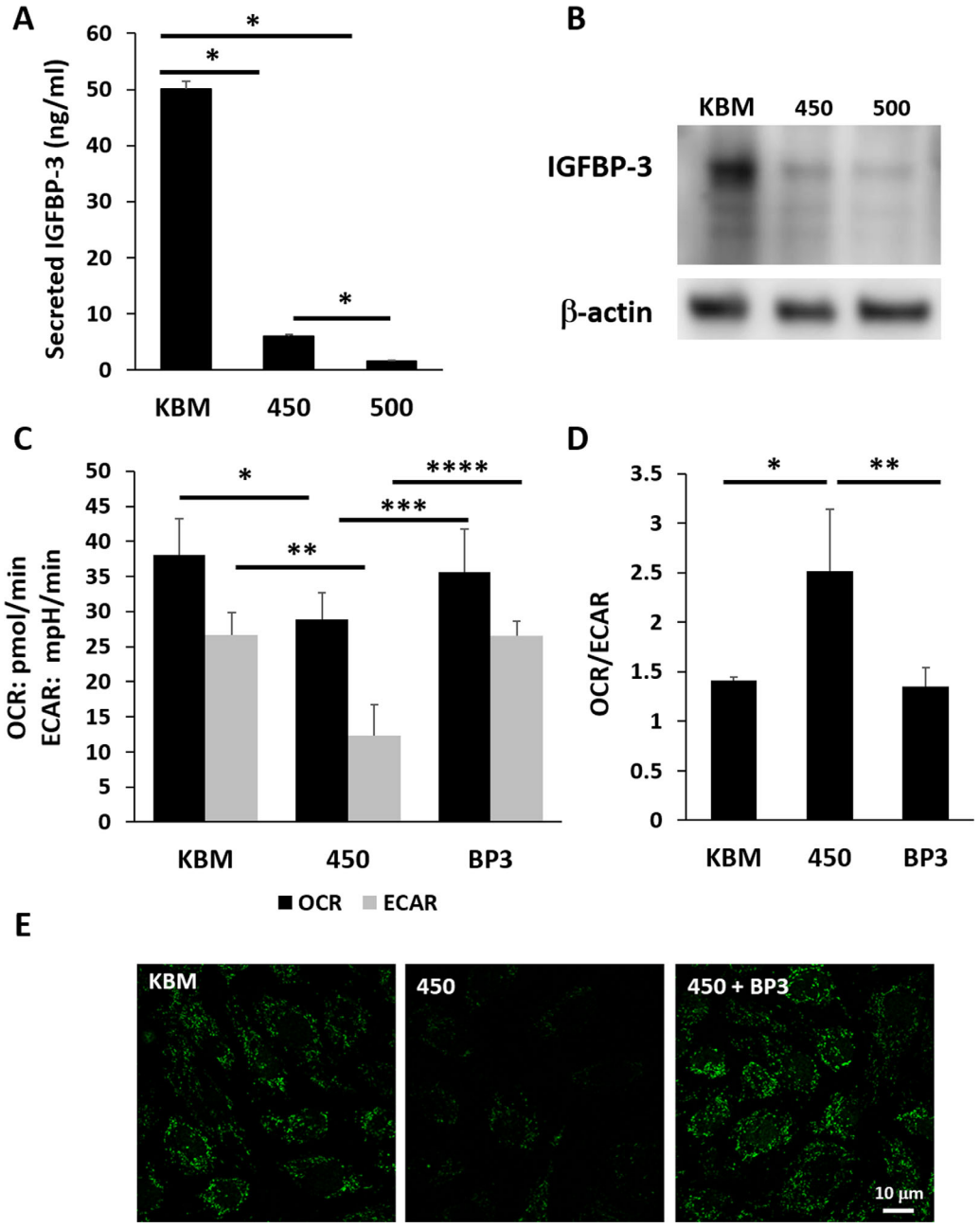

Figure 4. IGFBP-3 blocks the hyperosmolarity-induced decrease in mitochondrial respiration and glycolysis in corneal epithelial cells. The hTCEpi cells were cultured in basal media with or without hyperosmolar conditions for 24 hours. Cells cultured in 450 mOsM were cotreated with 500 ng/mL rhIGFBP-3. (**A**) IGFBP-3 secretion was down regulated in hyperosmolar culture in basal media ($^{*}P < 0.001$, one-way ANOVA, SNK multiple comparison test, n = 3). (**B**) Immunoblotting for intracellular IGFBP-3 in whole cell lysates. Consistent with the decrease in secreted IGFBP-3, intracellular IGFBP-3 was also sequentially decreased with increasing levels of salt. Beta-actin was used as a loading control. (**C**) Consistent with our prior results, both respiration and glycolysis were significantly decreased after culture in 450 mOsM/kg ($^{**}P = 0.021$ and $^{***}P = 0.011$, one-way ANOVA, SNK multiple comparison test, n = 3). Treatment with rhIGFBP-3 restored metabolism and glycolysis to basal levels ($^{****}P = 0.042$ and $^{*****}P = 0.012$, one-way ANOVA, SNK multiple comparison test, n = 3). (**D**) Hyperosmolar culture shifted cells toward a respiratory phenotype in hyperosmolar culture that was restored following treatment with rhIGFBP-3 ($^{******}P = 0.002$ and $^{*}P < 0.001$, one-way ANOVA, SNK multiple comparison test, n = 3). (**E**) SYBR green staining for mitochondrial DNA showed a decrease in mtDNA after hyperosmolar culture that was blocked by co-treatment with rhIGFBP-3. *Scale bar*: 10 µm. Number indicates mOsM. Images representative of three repeated experiments.

mitochondrial membrane polarization and caspase activation. Likewise, Deng et al.[22] measured levels of oxidative stress in primary cultured corneal epithelial cells and found an increase in reactive oxygen species and markers of oxidative damage. Together, these studies all highlight the negative impact of hyperosmolar stress in corneal epithelial cells on mitochondrial function.

Interestingly, there was a biphasic cell cycle response to hyperosmolar stress in basal media. This biphasic response was characterized by an early, acute hyperosmolar induced

Investigative Ophthalmology & Visual Science

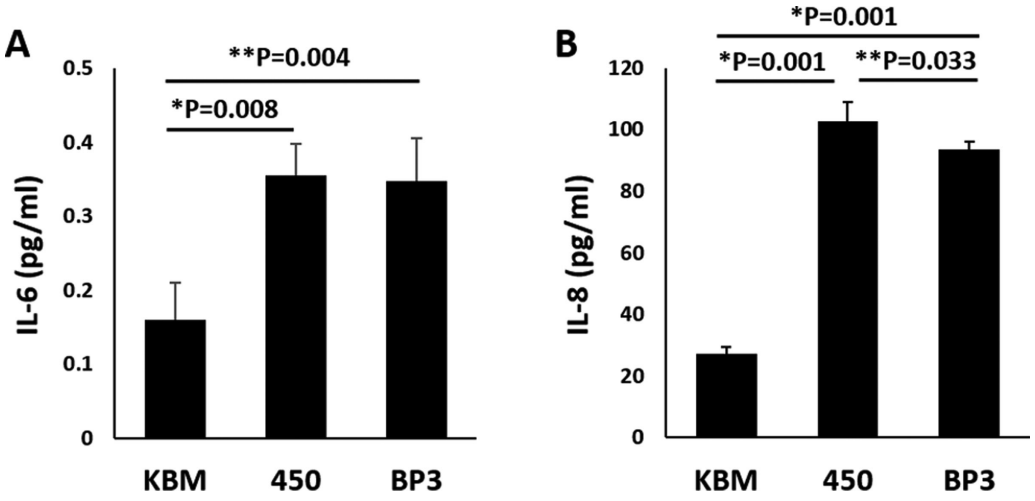

Figure 5. Hyperosmolar culture induced expression of the anti-inflammatory cytokines, IL-6 and IL-8. hTCEpi cells were cultured in basal media in isotonic and hyperosmolar conditions with and without 500 ng/mL rhIGFBP-3 for 24 hours. (**A**) Hyperosmolar culture triggered release of IL-6 that was not affected by treatment with rhIGFBP-3 ($^{*}P = 0.008$ for 450 compared to KBM, $^{**}P = 0.004$ for IGFBP-3 treated cells in hyperosmolar culture compared to KBM, one-way ANOVA, SNK multiple comparison test, n = 3). (**B**) IL-8 showed a more robust increase in hyperosmolar culture compared to KBM ($^{*}P = 0.001$). This increase was partially abrogated by treatment with rhIGFBP-3 ($^{**}P = 0.033$, one-way ANOVA, SNK multiple comparison test). Data represented as mean ± standard deviation.

cell cycle arrest at G2/M that was transient in nature. By 24 hours, cells were no longer arrested at G2/M and instead were beginning to accumulate in G0/G1. It is well established that metabolic changes and cell cycle control are bidirectional and osmotic stress has been shown to induce a transient cell cycle arrest in certain organisms.[56] This transient arrest is a counter-measure that mediates short term adaptation in response to stress and allows for a redistribution of the resources needed for survival. In contrast to this, the accumulation of cells at G0/G1 after 24 hours of hyperosmolar culture is most likely due to the higher energy demand required for cells to move into S phase. The decrease in ATP that is seen at this time point due to the attenuation in glycolysis and respiration is thus the rate limiting step essential for transition out of G0/G1.

The concentrations of salt tested in this study are consistent with other in vitro cell culture studies.[14–16,20–22,57] That being said, potential limitations exist when trying to extrapolate these findings to the in vivo ocular surface. Osmolarity is measured clinically by sampling tears that have pooled in the inferior tear meniscus. Indeed, early studies using this methodology have shown tear film osmolarity to range as high as 450 mOsM.[5] However, this may not reflect the true osmolarity across the corneal surface. More recent studies that have used psychophysical testing and mathematical modeling to predict tear film osmolarity in dry eye have yielded much higher values.[58,59] Moreover, the dynamics of the tear film during blinking and following tear break up may expose the corneal epithelium to transient spikes in osmolarity and may not be fully appreciated in a static in vitro hyperosmolar model. Thus additional studies are necessary to investigate the potential transient effects of hyperosmolarity on the corneal epithelium.

The concentration of salt aside, both salt concentrations induced IL-6 and IL-8 release by hTCEpi cells. This finding is consistent with work showing the upregulation of IL-6 and IL-8 under hyperosmolar conditions via aquaporin 5 and the transient receptor potential vanilloid 1 channel.[6,7] Unlike mitochondrial and metabolic effects however, rhIGFBP-3 was unable to block production of IL-6 and only partially blunted IL-8. Mitochondria are rapidly becoming recognized as signaling hubs for the innate immune system.[60,61] In the presence of stress, mitochondria release mtDNA into the cytosol.[62] We speculate that the reduction in mtDNA staining that was observed during hyperosmolar stress in this study may be due to cytosolic accumulation of mtDNA. This may contribute to uncontrolled inflammation that is present in dry eye disease. The potential to identify how IGFBP-3 or other mito-protective proteins may regulate inflammation through mtDNA release could represent a novel target for therapy.

In summary, hyperosmolar stress induces metabolic abnormalities, including the preferential decrease in glycolysis before the onset of mitochondrial damage. The reduction in glycolysis along with frank mitochondrial depolarization in turn attenuates mitochondrial respiration, resulting in reduced ATP production. Excitingly, the negative effects on both glycolysis and mitochondrial morphology and function are alleviated by exogenous IGFBP-3. Although further study is needed to determine the mechanism(s) by which IGFBP-3 mediates these effects, these findings support a new role for IGFBP-3 in the control of cellular metabolism.

Acknowledgments

Supported by NEI Grants R01 EY029258 (DMR), R01 EY024546 (DMR), T35 EY026510 (EB/DMR), F30 EY031559 (WLS), P30 EY030413, and an unrestricted grant from Research to Prevent Blindness, New York, NY.

Disclosure: **E.D. Bogdan,** None; **W.L. Stuard,** None; **R. Titone,** None; **D.M. Robertson,** None

References

1. Stapleton F, Alves M, Bunya VY, et al. TFOS DEWS II Epidemiology Report. *Ocul Surf.* 2017;15:334–365.

2. Craig JP, Nichols KK, Akpek EK, et al. TFOS DEWS II Definition and Classification Report. *Ocul Surf*. 2017;15:276–283.
3. Baudouin C, Aragona P, Messmer EM, et al. Role of hyperosmolarity in the pathogenesis and management of dry eye disease: proceedings of the OCEAN group meeting. *Ocul Surf*. 2013;11:246–258.
4. Shimazaki J. Definition and diagnostic criteria of dry eye disease: historical overview and future directions. *Invest Ophthalmol Vis Sci*. 2018;59:Des7–Des12.
5. Gilbard JP, Farris RL, Santamaria J, 2nd. Osmolarity of tear microvolumes in keratoconjunctivitis sicca. *Arch Ophthalmol*. 1978;96:677–681.
6. Pan Z, Wang Z, Yang H, Zhang F, Reinach PS. TRPV1 activation is required for hypertonicity-stimulated inflammatory cytokine release in human corneal epithelial cells. *Invest Ophthalmol Vis Sci*. 2011;52:485–493.
7. Ren Y, Lu H, Reinach PS, et al. Hyperosmolarity-induced AQP5 upregulation promotes inflammation and cell death via JNK1/2 Activation in human corneal epithelial cells. *Sci Rep*. 2017;7:4727.
8. Redfern RL, McDermott AM. Toll-like receptors in ocular surface disease. *Exp Eye Res*. 2010;90:679–687.
9. Lee HS, Hattori T, Park EY, Stevenson W, Chauhan SK, Dana R. Expression of toll-like receptor 4 contributes to corneal inflammation in experimental dry eye disease. *Invest Ophthalmol Vis Sci*. 2012;53:5632–5640.
10. Redfern RL, Patel N, Hanlon S, et al. Toll-like receptor expression and activation in mice with experimental dry eye. *Invest Ophthalmol Vis Sci*. 2013;54:1554–1563.
11. Redfern RL, Barabino S, Baxter J, Lema C, McDermott AM. Dry eye modulates the expression of toll-like receptors on the ocular surface. *Exp Eye Res*. 2015;134:80–89.
12. Shapiro L, Dinarello CA. Hyperosmotic stress as a stimulant for proinflammatory cytokine production. *Exp Cell Res*. 1997;231:354–362.
13. Luo L, Li DQ, Corrales RM, Pflugfelder SC. Hyperosmolar saline is a proinflammatory stress on the mouse ocular surface. *Eye Contact Lens*. 2005;31:186–193.
14. Li DQ, Luo L, Chen Z, Kim HS, Song XJ, Pflugfelder SC. JNK and ERK MAP kinases mediate induction of IL-1beta, TNF-alpha and IL-8 following hyperosmolar stress in human limbal epithelial cells. *Exp Eye Res*. 2006;82:588–596.
15. Zheng Q, Ren Y, Reinach PS, et al. Reactive oxygen species activated NLRP3 inflammasomes initiate inflammation in hyperosmolarity stressed human corneal epithelial cells and environment-induced dry eye patients. *Exp Eye Res*. 2015;134:133–140.
16. Chi W, Hua X, Chen X, et al. Mitochondrial DNA oxidation induces imbalanced activity of NLRP3/NLRP6 inflammasomes by activation of caspase-8 and BRCC36 in dry eye. *J Autoimmun*. 2017;80:65–76.
17. Li DQ, Chen Z, Song XJ, Luo L, Pflugfelder SC. Stimulation of matrix metalloproteinases by hyperosmolarity via a JNK pathway in human corneal epithelial cells. *Invest Ophthalmol Vis Sci*. 2004;45:4302–4311.
18. De Paiva CS, Corrales RM, Villarreal AL, et al. Corticosteroid and doxycycline suppress MMP-9 and inflammatory cytokine expression, MAPK activation in the corneal epithelium in experimental dry eye. *Exp Eye Res*. 2006;83:526–535.
19. Igarashi T, Fujimoto C, Suzuki H, et al. Short-time exposure of hyperosmolarity triggers interleukin-6 expression in corneal epithelial cells. *Cornea*. 2014;33:1342–1347.
20. Luo L, Li DQ, Pflugfelder SC. Hyperosmolarity-induced apoptosis in human corneal epithelial cells is mediated by cytochrome c and MAPK pathways. *Cornea*. 2007;26:452–460.
21. Png E, Samivelu GK, Yeo SH, Chew J, Chaurasia SS, Tong L. Hyperosmolarity-mediated mitochondrial dysfunction requires Transglutaminase-2 in human corneal epithelial cells. *J Cell Physiol*. 2011;226:693–699.
22. Deng R, Hua X, Li J, et al. Oxidative stress markers induced by hyperosmolarity in primary human corneal epithelial cells. *PloS One*. 2015;10:e0126561.
23. Julio G, Lluch S, Pujol P, Merindano MD. Effects of tear hyperosmolarity on conjunctival cells in mild to moderate dry eye. *Ophthalmic Physiol Opt*. 2012;32:317–323.
24. Ma S, Yu Z, Feng S, Chen H, Chen H, Lu X. Corneal autophagy and ocular surface inflammation: a new perspective in dry eye. *Exp Eye Res*. 2019;184:126–134.
25. Butt AJ, Williams AC. IGFBP-3 and apoptosis—a license to kill? *Apoptosis*. 2001;6:199–205.
26. Granata R, Trovato L, Garbarino G, et al. Dual effects of IGFBP-3 on endothelial cell apoptosis and survival: involvement of the sphingolipid signaling pathways. *FASEB J*. 2004;18:1456–1458.
27. Lee KW, Ma L, Yan X, Liu B, Zhang X-K, Cohen P. Rapid apoptosis induction by IGFBP-3 involves an insulin-like growth factor-independent nucleomitochondrial translocation of RXRa/Nur77. *J Biol Chem*. 2005;280:16942–16948.
28. Johnson MA, Firth SM. IGFBP-3: a cell fate pivot in cancer and disease. *Growth Horm IGF Res*. 2014;24:164–173.
29. Zhang Q, Jiang Y, Miller MJ, et al. IGFBP-3 and TNF-α regulate retinal endothelial cell apoptosis. *Invest Ophthalmol Vis Sci*. 2013;54:5376–5384.
30. Stuard WL, Titone R, Robertson DM. The IGF/insulin-IGFBP axis in corneal development, wound healing, and disease. *Front Endocrinol*. 2020;11:24.
31. Firth SM, Baxter RC. Cellular actions of the insulin-like growth factor binding proteins. *Endocr Rev*. 2002;23:824–854.
32. Baxter RC. Insulin-like growth factor binding protein-3 (IGFBP-3): Novel ligands mediate unexpected functions. *J Cell Commun Signal*. 2013;7:179–189.
33. Kelley KM, Oh Y, Gargosky SE, et al. Insulin-like growth factor-binding proteins (IGFBPs) and their regulatory dynamics. *Int J Biochem Cell Biol*. 1996;28:619–737.
34. Kim JH, Choi DS, Lee OH, Oh SH, Lippman SM, Lee HY. Antiangiogenic antitumor activities of IGFBP-3 are mediated by IGF-independent suppression of Erk1/2 activation and Egr-1-mediated transcriptional events. *Blood*. 2011;118:2622–2631.
35. Zhang Q, Soderland C, Steinle JJ. Regulation of retinal endothelial cell apoptosis through activation of the IGFBP-3 receptor. *Apoptosis*. 2013;18:361–368.
36. Oh Y, Müller HL, Pham H, Rosenfeld RG. Demonstration of receptors for insulin-like growth factor binding protein-3 on Hs578T human breast cancer cells. *J Biol Chem*. 1993;268:26045–26048.
37. Stuard WL, Titone R, Robertson DM. Tear levels of insulin-like growth factor binding protein 3 correlate with subbasal nerve plexus changes in patients with type 2 diabetes mellitus. *Invest Ophthalmol Vis Sci*. 2017;58:6105–6112.
38. Wu Y-C, Buckner BR, Zhu M, Cavanagh HD, Robertson DM. Elevated IGFBP3 levels in diabetic tears: a negative regulator of IGF-1 signaling in the corneal epithelium. *Ocul Surf*. 2012;10:100–107.
39. Zhu L, Titone R, Robertson DM. The impact of hyperglycemia on the corneal epithelium: molecular mechanisms and insight. *Ocul Surf*. 2019;17:644–654.
40. Titone R, Zhu M, Robertson DM. Insulin mediates de novo nuclear accumulation of the IGF-1/insulin Hybrid Receptor in corneal epithelial cells. *Sci Rep*. 2018;8:4378.
41. Kim SC, Hwang PH. Up-regulation of IGF Binding Protein-3 Inhibits Colonic Inflammatory Response. *J Korean Med Sci*. 2018;33:e110.

Investigative Ophthalmology & Visual Science

42. Lee YC, Jogie-Brahim S, Lee DY, et al. Insulin-like growth factor-binding protein-3 (IGFBP-3) blocks the effects of asthma by negatively regulating NF-κB signaling through IGFBP-3R-mediated activation of caspases. *J Biol Chem*. 2011;286:17898–17909.
43. Lee HS, Woo SJ, Koh HW, et al. Regulation of apoptosis and inflammatory responses by insulin-like growth factor binding protein 3 in fibroblast-like synoviocytes and experimental animal models of rheumatoid arthritis. *Arthritis Rheumatol*. 2014;66:863–873.
44. Robertson DM, Li L, Fisher S, et al. Characterization of growth and differentiation in a telomerase-immortalized human corneal epithelial cell line. *Invest Ophthalmol Vis Sci*. 2005;46:470–478.
45. Sasaki T, Sato Y, Higashiyama T, Sasaki N. Live imaging reveals the dynamics and regulation of mitochondrial nucleoids during the cell cycle in Fucci2-HeLa cells. *Sci Rep*. 2017;7:11257.
46. Titone R, Robertson DM. Insulin receptor preserves mitochondrial function by binding VDAC1 in insulin insensitive mucosal epithelial cells. *Faseb J*. 2020;34:754–775.
47. de RA, Jr. Glycolytic activity of the cornea. *AMA Arch Ophthalmol*. 1951;45:139–148.
48. Thies RS, Mandel LJ. Role of glucose in corneal metabolism. *Am J Physiol*. 1985;249:C409–416.
49. Morland C, Pettersen MN, Hassel B. Hyperosmolar sodium chloride is toxic to cultured neurons and causes reduction of glucose metabolism and ATP levels, an increase in glutamate uptake, and a reduction in cytosolic calcium. *Neurotoxicology*. 2016;54:34–43.
50. Wu YC, Buckner BR, Zhu M, Cavanagh HD, Robertson DM. Elevated IGFBP3 levels in diabetic tears: a negative regulator of IGF-1 signaling in the corneal epithelium. *Ocul Surf*. 2012;10:100–107.
51. Titone R, Zhu M, Robertson DM. Mutual regulation between IGF-1R and IGFBP-3 in human corneal epithelial cells. *J Cell Physiol*. 2019;234:1426–1441.
52. Wu YC, Zhu M, Robertson DM. Novel nuclear localization and potential function of insulin-like growth factor-1 receptor/insulin receptor hybrid in corneal epithelial cells. *PloS one*. 2012;7:e42483.
53. Warsito D, Sjöström S, Andersson S, Larsson O, Sehat B. Nuclear IGF1R is a transcriptional co-activator of LEF1/TCF. *EMBO Rep*. 2012;13:244–250.
54. Sarfstein R, Werner H. Minireview: nuclear insulin and insulin-like growth factor-1 receptors: a novel paradigm in signal transduction. *Endocrinology*. 2013;154:1672–1679.
55. Sehat B, Tofigh A, Lin Y, et al. SUMOylation mediates the nuclear translocation and signaling of the IGF-1 receptor. *Sci Signal*. 2010;3:ra10.
56. Bonny AR, Kochanowski K, Diether M, El-Samad H. Stress-induced transient cell cycle arrest coordinates metabolic resource allocation to balance adaptive tradeoffs. bioRxiv. 2020.
57. Yang L, Zhang S, Duan H, et al. Different effects of pro-inflammatory factors and hyperosmotic stress on corneal epithelial stem/progenitor cells and wound healing in mice. *Stem Cells Transl Med*. 2019;8:46–57.
58. Braun RJ, King-Smith PE, Begley CG, Li L, Gewecke NR. Dynamics and function of the tear film in relation to the blink cycle. *Prog Retin Eye Res*. 2015;45:132–164.
59. Peng CC, Cerretani C, Braun RJ, Radke CJ. Evaporation-driven instability of the precorneal tear film. *Adv Colloid Interface Sci*. 2014;206:250–264.
60. Breda CNS, Davanzo GG, Basso PJ, Saraiva Câmara NO, Moraes-Vieira PMM. Mitochondria as central hub of the immune system. *Redox Biol*. 2019;26:101255.
61. Sandhir R, Halder A, Sunkaria A. Mitochondria as a centrally positioned hub in the innate immune response. *Biochim Biophys Acta Mol Basis Dis*. 2017;1863:1090–1097.
62. Aarreberg LD, Esser-Nobis K, Driscoll C, Shuvarikov A, Roby JA, Gale M, Jr. Interleukin-1β Induces mtDNA Release to Activate Innate Immune Signaling via cGAS-STING. *Mol Cell*. 2019;74:801–815.e806.

Investigative Ophthalmology & Visual Science